
**Separation Science and Technology**
Publication details, including instructions for authors and subscription information:
http://www.informaworld.com/smpp/title~content=t713708471

# A Comprehensive Characterization of Commercial Nanofiltration Membranes

Gamze Artuğ[a]; Indriana Roosmasari[a]; Klaus Richau[b]; Jobst Hapke[a]
[a] Department of Plant Design, Technical University Hamburg-Harburg, Hamburg, Germany [b] GKSS Research Centre Geesthacht GmbH, Institute of Chemistry, Teltow, Germany

**To cite this Article** Artuğ, Gamze , Roosmasari, Indriana , Richau, Klaus and Hapke, Jobst(2007) 'A Comprehensive Characterization of Commercial Nanofiltration Membranes', Separation Science and Technology, 42: 13, 2947 — 2986
**To link to this Article: DOI:** 10.1080/01496390701560082
**URL:** http://dx.doi.org/10.1080/01496390701560082

*Separation Science and Technology*, 42: 2947–2986, 2007

ISSN 0149-6395 print/1520-5754 online
DOI: 10.1080/01496390701560082



# A Comprehensive Characterization of Commercial Nanofiltration Membranes

**Gamze Artuğ and Indriana Roosmasari**
Department of Plant Design, Technical University Hamburg-Harburg, Hamburg, Germany

**Klaus Richau**
GKSS Research Centre Geesthacht GmbH, Institute of Chemistry, Teltow, Germany

**Jobst Hapke**
Department of Plant Design, Technical University Hamburg-Harburg, Hamburg, Germany

**Abstract:** This paper presents a comprehensive characterization study of NF 90 (Filmtec), NF 270 (Filmtec), NF 2 (Sepro), and NF PES 10 (Microdyn-Nadir) membranes by their morphology, charge, and separation performance parameters. Extensive investigations of the relations between membrane performance and membrane charge/morphological properties were performed by various measurement methods and active layer mass transport modelling. For this purpose, a broad experimental program was exerted with saccharides and polyethylene glycol at various pressures and with single salt solutions of NaCl, $CaCl_2$, $Na_2SO_4$, and $MgSO_4$ at various concentrations. pH effect on membrane performances was investigated as well. A Fortran program code of a hydrodynamic model was developed in order to determine the pore sizes of the membranes using the experimental data with organics. In addition, an equation-based software, COMSOL Multiphysics, was utilized for the modelling with salt solutions. This eliminated the effort demanding program code writing for concentration and potential differential equations derived from extended Nernst-Planck (ENP) equation, which is a common method in many publications. By this model, transport phenomena inside the membrane, relation

Received 19 July 2006, Accepted 10 October 2006
Address correspondence to Gamze Artuğ, Department of Plant Design, Technical University Hamburg-Harburg, Eissendorfer Strasse 38, Hamburg 21073, Germany. Tel.: +49-40-537-92-282; E-mail: gamze_artug@yahoo.com

between the membrane performance and its charge, as well as performance prediction of the membranes could be quested in detail.

**Keywords:** Nanofiltration, characterization, morphology, charge, modelling, performance prediction

## INTRODUCTION

Nanofiltration (NF) is positioned between ultrafiltration and reverse osmosis in respect of the pressures applied in a process and its separation range. In addition, different from other membranes, charge is a unique property for NF membranes. Consequently, apart from steric effects, electrical effects can be decisive for the separation behavior. Owing to its characteristics, NF has a flexible application area in various industries especially for the removal of salts and small molecules. Some of them are filtration of paper mill total effluent (1, 2), demineralization in the dairy industry (3, 4), in wastewater treatment (5–7), and recently as a new approach in the pre-treatment of seawater in desalination plants (8, 9).

Membrane characterization has become almost a standard method prior to new applications, to enhance the process efficiency, to identify the background rejection mechanisms for the separation performance, as well as in research and development studies of membrane materials. NF industrial fields under investigation such as pharmaceutical industry and surface and wastewater treatment for the removal of endocrine disrupting compounds, pharmaceutically active compounds, and personal care products are some examples where characterization study is of paramount importance to improve the process efficiency. The rejection mechanisms behind the separation performance in these applications are rather complicated due to the solutes with quite distinct physicochemical properties as well as solution chemistry and their interactions with membranes. Consequently, relatively more comprehensive characterization studies are applied. Some examples are highlighted in (5, 10–12). It was pointed out the rare use of NF in water recycle applications due to the lack of information considering the relationship of solution chemistry, physicochemical properties of the trace organics (size, dipole moment), membrane pore size, and charge to the retention (5). Nghiem et al. (5) elucidated the transport mechanisms in the removal of trace pharmaceuticals by using NF 90 and NF 270 membranes. Retentions of negatively charged pharmaceuticals could be improved at high solution pH for NF 270 membrane owing to its acidic character. As the solution pH decreased, electrostatic repulsion between NF 270 and ibuprofen (carboxylic groups) decreased and adsorption increased. In the case of NF 90 membrane, retentions were controlled by steric effects. For this membrane, lower pore size was determined. This study demonstrated the importance of various effects in rejection mechanisms and the ease of understanding of them by means of

solute, solution, and membrane characteristics. Another example is the pulp and paper industry, which explores the hydrophobic character of the membranes since this property plays an important role in system performance in terms of its contributions to fouling. To summarize, characterization studies and understanding the mechanisms behind the membrane performance can be utilized to enhance the process efficiency. Examples to improve process efficiency can be the adjustment of solution pH or the use of charge interactions between the membrane and the charged components to separate charged from neutral and/or oppositely charged components. The mechanisms behind membrane performance will be explored in this paper.

In addition, the widely used transport mechanistic-based models necessitate structure and performance parameters of a membrane and thus address a characterization study. Consequently, modelling for the membrane performance description and prediction is another challenge for the membrane characterization. Bowen and Mohammed (13, 14) made an analysis for a number of commercially available NF membranes for the processing of dye/salt/water streams by using the Donnan-Steric-Pore model (DSPM), developed by Bowen et al. (15). The model considers the membrane as porous, utilizes ENP equation, and necessitates three membrane parameters; namely, effective pore radius, effective membrane thickness to porosity ratio, and effective membrane charge density. They found out that when the removal of salt in dye/salt solution is considered through diafiltration, in which the process requires complete retention of dye with low retentions of sodium and chloride ions, a membrane with a pore size smaller than the effective radius of the dye molecule is a good choice. Membranes with low charge were found to be favorable for the process since they resulted in negative rejections for chloride ions. They also ascertained that a low membrane thickness value shortens the process time. Consequently, the model enabled the specification of the membrane properties for the related process. In another work of Bowen and Mohammed (16), DSPM, incorporated with concentration polarization effect, was used for the characterization of the membranes, which enabled the predictions of the rejections at different dye solution concentrations as well as the further optimization of the process in terms of the membrane's structural and electrical properties. Subsequently, membrane characterization along with modelling testifies a selective tool for an appropriate membrane regarding the related process and bears out for a prediction and an optimization tool.

Charge of a NF membrane is a peculiar property in terms of its effects on the separation behavior. It is strongly correlated to species transport through the boundary layer and within the membrane itself. Consequently, it becomes essential to understand the charge behavior of a NF membrane to attain the highest performance in a process. NF membranes acquire an electrical charge by a number of mechanisms. When they get in contact with an electrolyte solution, the functional groups of a membrane dissociate depending on the pH of the solution. Other mechanisms are adsorption of ions from solution,

adsorption of polyelectrolytes, ionic surfactants, and charged macromolecules (17, 18).

The strong dependency of the charge and thus the separation performance on the feed concentration (13, 16, 18–24), the type of the salt (18–23), and the pH of the solution (18, 24–26) is confirmed in many studies. Teixeira et al. (18) detected a decrease in flux and an increase in rejection of salts by increasing pH. They also observed an increase in uncharged solute rejection with membrane charge. This was ascribed to the structural changes in membrane with the increase in negatively charged groups, which resulted in an extended structure and reduced pore size. Peeters et al. (23) performed streaming potential measurements for different single salts at different concentrations. The calculation of kinetic surface charge densities indicated that the surface charge density is dependent on anion concentration rather than the solution concentration itself. As anions are less hydrated in the neighborhood of non-polar surfaces than cations, they can adsorb more easily to the surface, resulting in an excessive negative charge (27, 28). In view of the rejection performance with charged components, the membrane with a higher surface charge density proved Donnan exclusion, whereas the one with a lower surface charge density exhibited a combination of Donnan and steric exclusion mechanisms. Bandini et al. (29) observed higher rejection values at increasing pH at a constant concentration. Moreover, at a constant pH as the electrolyte concentration increased, rejection decreased. This was assigned to the increased membrane charge and the more dominant Donnan effect on counterion, which also enhanced the permeation of salt due to electroneutrality condition. Berg et al. (19) attributed this decline in rejection to the decreasing ratio of the membrane charge to feed concentration as the feed concentration increased. This is ascribed to the adherence of more cations to the membrane functional groups. Hence, despite the increasing membrane charge density, electrostatic interactions and consequently rejection decreased with an augmenting feed concentration. The dependency of the membrane charge on several factors as mentioned above gives rise to a much more complicated modelling for NF in comparison to the other membrane processes.

Over the past 10 years, there has been a growing realization of physical models (13–16, 19, 20, 22, 25, 30, 31). Some enhancements of the phenomenological models (32, 33) for NF membranes have been published as well. The most currently used NF models are based on ENP equation, which describes the transport of an ion across the membrane by diffusion due to concentration gradient, migration due to electrical potential gradient and convection caused by the pressure difference. Distribution of ions at the membrane-solution interface results from various mechanisms. This distribution is expressed through the Donnan-steric partitioning in this work. In the modelling part of this work, the ENP equation along with the Donnan-steric partitioning ion distribution at the interfaces is utilized.

The objective of this study is to contribute to the understanding of NF performance by characterizing four commercially available NF membranes.

Having started with morphology investigations by microscopy and contact angle measurements as well as charge investigations by electrokinetic measurements, a systematic experimental program with pure water, organic and salt solutions were applied. Apart from experimental means, a general practical tool is aimed to be developed for the membrane characterization and performance prediction purposes in a user friendly software which can be applied to various component systems. Unlike previous studies, where the differential equations for the concentration and the potential gradients are first derived from the ENP equation and solved by the Runga-Kutta-Gill method, in this study COMSOL Multiphysics software was utilized which eliminated writing a program code and allowed straightforward modifications for the regarded feed stream. The software provides an equation-based modelling and has a large number of ready-to-use application modes. In this study, Nernst-Planck application and Darcy's Law application modes were used. The software with its multiphysics feature enabled the coupling of momentum and mass balances. It has a flexible model set-up that provides discrete implementation of boundary conditions from the main equation system. Therefore, it is easily adoptable for various component systems. Its modelling environment consists of setting up the geometry, defining physics (modifying the equations, setting domain properties, constants, expressions, and boundary conditions), creating a mesh (automatic mesh generation), solving the model by its solvers, and performing post-processing (visualization and analysis of results).



## MATERIALS AND METHODS

### Membranes

Flat sheet samples were used. Attention is given to industrially favorable polymeric membranes covering different structures and application ranges. The characteristics of the membranes are tabulated in Table 1. NF 90, NF 270 and NF 2 are TFC membranes in which, the ultrathin active layer is based on a microporous polysulphone interlayer (40 μm) and a polyester non-woven support web (120 μm) (34). NF PES 10 is made of a permanently hydrophilic polyethersulphone-polyvinylpromidone copolymer on a polypropylene support. NF 90 is an aromatic polyamide, which contains carboxylic acid and primary amines ($-NH_2$), whereas NF 270 is a mixed aromatic, aliphatic polyamide (polypiperazine amide) with secondary amine (-NH) and carboxylic acids (34). Carboxylic acids are weak acids and the acidity increases in the presence of electronegative groups such as -OH, -Cl. The different dissociation constants of piperazine result in different salt selectivity at different applications (34). Some test data from the manufacturers are tabulated in Table 2.

***Table 1.*** Membrane manufacturer data

| Manufacturer | Membrane | Material | Cut-off (g/mol) | $P_{max}$ (MPa) | $T_{max}$ (°C) | pH |
|---|---|---|---|---|---|---|
| DOW Filmtec | NF 90 | Polyamide, TFC | 200–300 | 4.1 | 45 | 3–10 |
| DOW Filmtec | NF 270 | Polypiperazine amide, TFC | 200–300 | 4.1 | 45 | 3–10 |
| Sepro | NF 2 | Polyamide, TFC | 300–400 | 4.4 | 50 | 3–10 |
| Microdyn-Nadir | NF PES 10 | Polyethersulphone, IA | 1000 | 4.0 | 94 | 0–14 |

TFC = Thin film composite, IA = Integrally asymmetric, $P_{max}$ = maximum pressure, $T_{max}$ = maximum temperature.

***Table 2.*** Test data of membranes delivered by manufacturers

| Membrane | $P$ (MPa) | $T$ (°C) | System | $A$ ($m^2$) | $J_P$ ($L/(m^2\ h)$) | Salt | $C_F$ (ppm) | $R$ (%) |
|---|---|---|---|---|---|---|---|---|
| NF 90 | 0.48 | 25 | SWM | 37 | 32 | NaCl | 2000 | 85–95 |
| | | | | | 41 | $MgSO_4$ | 2000 | >97 |
| NF 270 | 0.48 | 25 | SWM | 37 | 63 | $CaCl_2$ | 500 | 40–60 |
| | | | | | 53 | $MgSO_4$ | 2000 | >97 |
| | 0.9 | n.s | Flat channel | n.s | 122–167 | $MgSO_4$ | 2000 | 99.2 |
| NF 2 | 1.03 | 25 | n.s | n.s | 135 | $MgSO_4$ | 2000 | 98 |
| NF PES 10 | 4.0 | 20 | Stirred cell | n.s | 200–400 | NaCl | n.s | 5–15 |
| | | | | | | $Na_2SO_4$ | | 30–60 |

A = Membrane area, SWM = spiral-wound module, n.s = not stated.

## Cross-flow Flat Channel

Permeation experiments were conducted in a cross-flow flat channel test cell with a membrane area of 274 $cm^2$. A 44 mil parallel feed spacer was used in all experiments, which brought a channel height of 1.3 mm. All the experiments were performed at a circulating flow rate of 234 L/h, which refers to a 1.1 m/s cross-flow velocity in channel. Experiments were carried out in circulation mode. Thus, feed concentration is assumed to be constant.

## Chemicals

Saccharides (glucose, sucrose, raffinose) and polyethylene glycol (PEG 1000) for the organic rejection measurements, whereas NaCl (1-1), $Na_2SO_4$ (1-2), $MgSO_4$ (2-2), and $CaCl_2$ (2-1) salts for the single salt rejection measurements were used. Solutions were prepared by deionized water, which has conductivity less than 9 μS/cm. Table 3 lists the properties of organics and ions.

## Experimental Procedures

A new membrane sample was used for each experiment. The pure water permeability measurements were performed at varying pressures between 0.3 to 1.3 MPa at 20°C. At first, the membrane sample was filtered with deionized water without circulating retentate and permeate back to the feed tank so that impurities were washed out from the system. Afterwards, the system was put in circulation mode, pressurized to 1.3 MPa, and the temperature was let to increase. Approximately 30 minutes later, the operating conditions were set. Having waited circa 40–60 minutes, the first measurement was done at which the permeate flux was measured and the pressure, temperature, flow

***Table 3.*** Stokes radius $r_S$ and diffusivities $D_i$ of organic solutes and ions (35, 36)

| Organic/ion | MW (g/mol) | $r_S$ (nm) | $D_i$ ($10^{-9}$ $m^2/s$) |
|---|---|---|---|
| Glucose | 180.16 | 0.324 | 0.658 |
| Sucrose | 342.30 | 0.419 | 0.501 |
| Raffinose | 594.51 | 0.500 | 0.421 |
| PEG 1000 | 1000 | 0.94 | 0.309 |
| $Mg^{2+}$ | 24.31 | 0.347 | 0.706 |
| $Ca^{2+}$ | 40.08 | 0.310 | 0.920 |
| $Na^{+}$ | 22.99 | 0.184 | 1.334 |
| $SO_4^{2-}$ | 96.06 | 0.230 | 1.065 |
| $Cl^{-}$ | 35.45 | 0.121 | 2.032 |

MW = Molecular weight.

rate, and the pressure difference were recorded. After 20 minutes, a second measurement was conducted. When the flux reached a stable value, the new pressure was set and measurements were repeated. By this method, pure water permeability measurements were executed in 3 runs for NF 270 membrane: first from 1.0 to 0.3 MPa down then to 1.0 MPa up and again to 0.3 MPa down. Membrane constant was determined from the slope of the flux curve plotted as a function of the transmembrane pressure difference. In this manner, no occurrence of membrane compaction is confirmed in the studied pressure range. From the last 2 runs, almost the same permeabilities were obtained. Thus the measurements were restricted to the first 2 runs for the other membranes. Measurements for NF 90 and NF 2 membranes were repeated for different samples to check the reproducibility of the results.

Organic rejection measurements were conducted at varying pressures of 0.3, 0.5, 0.8, and 1.0 MPa and at 20°C. The feed concentrations set were around 430 ppm. Raffinose and PEG 1000 were used for NF PES 10 experiments due to the relatively higher MWCO of this membrane and saccharides for TFC membranes. Membrane was first conditioned with deionized water. The stabilization time of approximately 40–60 minutes was waited and pure water permeability was measured at 1.0 MPa. A stable value was achieved after around 30 minutes. Similar preparation method of NF membranes at 9 bar around 2 hours was applied in (33) as well. Afterwards, prepared organic solution was added to the system. The pressure was set to 0.3 MPa. 30 minutes later, flux measurements were performed as described in the previous section. Measurement was repeated 20 minutes later and if the flux values from both measurements were close, samples were taken from feed and permeate streams for the concentration determinations in the laboratory. By doing this, measurements were conducted further at 0.5, 0.8, and 1.0 MPa.

Salt solution experiments as a function of concentration were performed at 1.0 MPa, 20°C, pH around 5.5–7. The set concentrations were 0.003 M, 0.01 M, 0.03 M, and 0.1 M. Specifically, NaCl concentration varied between 175 to 6000 ppm, $CaCl_2$ between 400–15,000 ppm, $Na_2SO_4$ between 400 to 15,000 ppm, and $MgSO_4$ between 400 to 14,000 ppm. After membrane conditioning with deionized water, the pure water permeability was measured. Thereafter, the feed concentration was set. Approximately 60 minutes were waited for the stabilization. Flux and rejection measurements were conducted at the first concentration point. Measurements were repeated 15–20 minutes later. By this procedure, mostly two measurement points were enough at a set concentration. Then, the new concentration was adjusted.

At the end of the experiments with organic and salt solutions, pure water flux was measured again to determine the flux decline and thus the fouling tendency of the membranes.

In addition, experiments for the investigation of pH effect were conducted in the acidic pH range of 2–7 for the selected membranes and salts starting from high to lower pH values by stepwise addition of HCl to the feed

solution. Operating conditions were 1.0 MPa, 20°C and 234 L/h. The experimental procedure was similar to the previous ones. At each pH measurement point, samples were taken from the feed and permeate streams for concentration determinations.

## Analysis

Concentrations were determined by HPLC RI detector (Agilent G1362A) for organics and by a conductivity meter Inolab Multi level 3 (WTW-Germany) with TetraCon 325 electrode (1 μS/cm to 2 S/cm with a deviation of ±0.5%) for salts. The flux of the permeate stream was measured by weighing the mass in time by a laboratory balance Sartorius CP 4202 S (0–4200 g, deviation ±0.01 g of displayed value). pH measurements were conducted by SenTix®81 sensor (0–14 pH with a deviation of ±0.01 pH). Samples of pH experiments were analyzed to determine cation concentrations by using PE Optima 2000 DV Optic Emissions Spectroscopy (OES) with Inductive Coupled Plasma (ICP) method.



## Contact Angle Measurements

Contact angle measurements were performed in order to investigate hydrophilic/hydrophobic character of the membranes. For this purpose, sessile drop (1) and captive bubble measurements were conducted with the equipment provided by Zeiss, Germany. In addition, more sessile drop (2) measurements were conducted with G-1 Contact Anglemeter from Erma Inc., Japan.

## AFM Analysis

Atomic Force Microscopy (AFM) (NanoScope IIIA) was applied to determine the surface roughnesses of the membranes. Measurements were conducted at contact mode.

## Tangential Streaming Potential Measurements

These measurements were performed using an electrokinetic analyzer (Anton Paar K.G., Austria). For KCl salt (0.005 M), in the first run, the pH was changed stepwise down to pH 3 and in the second run towards alkaline pH. Measurements were conducted with at 25°C. For NaCl and $CaCl_2$ solutions, measurements were performed only in acidic range at four different concentrations: 0.3, 0.75, 1, and 3 mol/$m^3$ and at 24°C.

## THEORY

Active layer NF transport as well as partitioning at membrane interfaces is of concern in the modelling. Typical profiles of concentrations and potential as well as transport mechanisms in a negatively charged NF membrane are presented in Fig. 1. The system is considered at steady state and the experimental data, taken at steady state conditions, are used in simulations.

The domain geometry in the program is visualized in 2D for the ease of implementation, the decisive coordinate is x though. The geometry presents the cross section of active layer (Fig. 1). At first, constants and expressions which are donated in Table 4 and Table 5 are set in the program.

Essential parameters for the modelling purposes are categorized in three groups: membrane parameters, solute/solution properties, process parameters. Pore radii and porosities of the membranes are determined by means of the



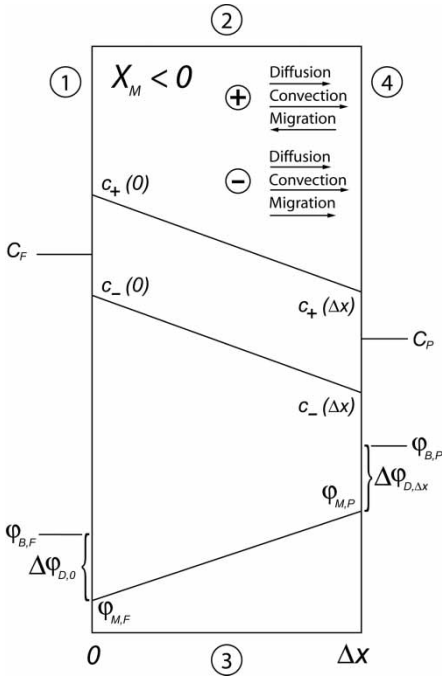


***Figure 1.*** The simplified illustration of concentrations (feed concentration $C_F$, permeate concentration, $C_P$, feed side positive and negative ion concentrations inside the membrane $c_+(0)$, $c_-(0)$, permeate side positive and negative ion concentrations inside the membrane $c_+(\Delta x)$, $c_-(\Delta x)$), potential (potential in feed bulk, $\varphi_{B,F}$, potential in permeate bulk, $\varphi_{B,P}$, potential in membrane on feed side, $\varphi_{M,F}$, potential in membrane on permeate side, $\varphi_{M,P}$, Donnan potential at feed side, $\Delta\varphi_{D,0}$, Donnan potential at permeate side, $\Delta\varphi_{D,\Delta x}$) profiles and transport mechanisms inside a negatively charged ($X_M < 0$) nanofiltration membrane. The notations 1, 2, 3, 4 (interfaces of the membrane) refer to the boundary conditions mentioned in Section 3.2.

method, which will be introduced in the following. Membrane constant is calculated from the pure water permeability measurements. Membrane thickness is regarded as the swollen active layer thickness. The swollen active layer thickness of the NF 270 membrane was determined as 19 nm from AFM study in (37), which is also used in the simulations performed in this work. NF 200 was about twice as thick and NF 270 was twice as permeable as NF 200 (37). Based on the inverse relation between the active layer thickness and permeability, the thicknesses of the TFC membranes in our work were approximated as 26 nm for NF 90 and 20 nm for NF 2. NF PES 10 thickness is determined from the SEM view in (11) as 20 nm. Membrane charge is expressed as a function of feed concentration by solving the equation systems, the implementation of which in COMSOL Multiphysics is introduced in the following sections (Table 6).



## Effective Pore Radius and Porosity Determinations

The model equations and the method for the determination of the pore radius by using the uncharged solute rejection data have already been explored and

***Table 4.*** Constants used in the program

| Constants | Unit |
|---|---|
| Gas constant $*$ temperature ($R_gT$) | J/mol |
| Pore size ($r_s$) | m |
| Ion 1 charge ($z_1$) | — |
| Ion 2 charge ($z_2$) | — |
| Feed concentration ($C_F$) | $mol/m^3$ |
| Membrane charge ($X_M$) | $mol/m^3$ |
| Size of ion 1 ($r_1$) | m |
| Size of ion 2 ($r_2$) | m |
| Bulk diffusivity of ion 1 ($D_1$) | $m^2/s$ |
| Bulk diffusivity of ion 2 ($D_2$) | $m^2/s$ |
| Density of solution ($\rho$) | $kg/m^3$ |
| Thickness of the oriented solvent layer ($d$) | m |
| Electronic charge ($e$) | C |
| Permittivity of free space ($\varepsilon_o$) | $C^2/(J\ m)$ |
| Boltzman constant ($k_B$) | J/K |
| Water dielectric constant ($\varepsilon_b$) | — |
| Faraday constant ($F$) | C/mol |
| Feed pressure ($P_F$) | Pa |
| Permeate concentration ($C_p$) | $mol/m^3$ |
| Permeate water velocity ($J_W$) | m/s |
| Porosity ($\varepsilon$) | — |
| Permeability ($k$) | $m^2$ |
| Membrane constant ($L_P$) | m/(s Pa) |

***Table 5.*** Expressions used in the program

| Expressions | Unit |
|---|---|
| Ratio of ion 1 to pore radius ($\lambda_1$) | — |
| Ratio of ion 2 to pore radius ($\lambda_2$) | — |
| Steric partition coefficient for ion 1 ($\phi_1$) | — |
| Steric partition coefficient for ion 2 ($\phi_2$) | — |
| Diffusion hindrance factor for ion 1 ($K_{d,1}$) | — |
| Diffusion hindrance factor for ion 2 ($K_{d,2}$) | — |
| Viscosity in pore ($\eta$) | Pa s |
| Pore diffusivity for ion 1 ($D_{1,P}$) | $m^2/s$ |
| Pore diffusivity for ion 2 ($D_{2,P}$) | $m^2/s$ |
| Concentration of ion 2 at the pore inlet (($c_2$0)) | $mol/m^3$ |
| Concentration of ion 2 at the pore outlet ($c_2(\Delta x)$) | $mol/m^3$ |

applied in several works and gave excellent predictions (14, 21, 30). In this method, rejection is derived as:

$$R_{calc} = 1 - \frac{\phi}{1 - (1 - \phi) \cdot \exp(-Pe)} \tag{1}$$

***Table 6.*** Equation system for Nernst-Planck Application mode with n number of components

| Term | Equations |
|---|---|
| $\Gamma_x$ | $-F\left(\sum_{i=1}^{n} z_i D_{xx_{i,P}} \frac{\partial c_i}{\partial x} + \sum_{i=1}^{n} z_i D_{xy_{i,P}} \frac{\partial c_i}{\partial y} + \sum_{i=1}^{n} z_i^2 u_i F c_i \frac{\partial \varphi}{\partial x} - V_x(-X_M)\right)$ $-\left(D_{xx_{2,P}} \frac{\partial c_2}{\partial x} + D_{xy_{2,P}} \frac{\partial c_2}{\partial y} + z_2 u_2 F c_2 \frac{\partial \varphi}{\partial x}\right)$ : $-\left(D_{xx_{n,P}} \frac{\partial c_n}{\partial x} + D_{xy_{n,P}} \frac{\partial c_n}{\partial y} + z_n u_n F c_n \frac{\partial \varphi}{\partial x}\right)$ |
| $\Gamma_y$ | $-F\left(\sum_{i=1}^{n} z_i D_{yx_{i,P}} \frac{\partial c_i}{\partial x} + \sum_{i=1}^{n} z_i D_{yy_{i,P}} \frac{\partial c_i}{\partial y} + \sum_{i=1}^{n} z_i^2 u_i F c_i \frac{\partial \varphi}{\partial y} - V_y(-X_M)\right)$ $-\left(D_{yx_{2,P}} \frac{\partial c_2}{\partial x} + D_{yy_{2,P}} \frac{\partial c_2}{\partial y} + z_2 u_2 F c_2 \frac{\partial \varphi}{\partial y}\right)$ : $-\left(D_{yx_{n,P}} \frac{\partial c_n}{\partial x} + D_{yy_{n,P}} \frac{\partial c_n}{\partial y} + z_n u_n F c_n \frac{\partial \varphi}{\partial y}\right)$ |
| $S$ | $0 - \left(V_x \frac{\partial c_2}{\partial x} + V_y \frac{\partial c_2}{\partial y}\right)$ : $- \left(V_x \frac{\partial c_n}{\partial x} + V_y \frac{\partial c_n}{\partial y}\right)$ |

*Pe* is the peclet number:

$$Pe = \frac{V\Delta x}{D_P} \tag{2}$$

where $V$ is the solvent velocity in the membrane and described by the Hagen-Poiseuille equation:

$$V = \frac{r_p^2 \Delta P_e}{8\eta\Delta x} \tag{3}$$

$D_p$ in Eq. (2) and $\eta$ in Eq. (3) are defined in membrane pores (21) as:

$$D_P = D \cdot K_d \cdot \frac{\eta_0}{\eta} \tag{4}$$

$$\eta = \eta_0 \cdot \left(1 + 18\left(\frac{d}{r_p}\right) - 9\left(\frac{d}{r_p}\right)^2\right) \tag{5}$$

$\phi$ is the steric partition coefficient defined as (15):

$$\phi = (1 - \lambda)^2 \tag{6}$$

and $\lambda$ is:

$$\lambda = \frac{r_S}{r_P} \tag{7}$$

An iteration program was written in Fortran 90 programming code. The feed and permeate concentrations along with the effective driving pressures in the experiments are inputs. The program iterates the pore size till the calculated and the measured rejection values agree in the given error range.

Assuming that inside the membrane, pores are arranged as parallel cylinders, applying continuity equation, the permeate water flux can be correlated to the average velocity inside the pore as:

$$J_W = V \cdot \varepsilon \tag{8}$$

Consequently, the porosity can be calculated by using the experimental data and the Hagen-Poiseuille equation provided that the pore size and membrane thickness are known and the support layer porosity along with its transport resistance are neglected.

## Modelling of Ion Transport in Nanofiltration Membranes

A combination of the Tsuru model (19) and DSPM (15) is implemented in COMSOL Multiphysics in the view that hindrance factors for diffusion are taken into account (DSPM) and mobility in the pore is assumed to be the

same as in the bulk (Tsuru model). Application of physical models entails a number of assumptions:

- same activity coefficients are assumed in membrane and bulk, $\gamma_i^M/\gamma_i = 1$, where the activity coefficients in bulk is set to 1 (Tsuru model) so that the solution is assumed diluted
- membrane is electrically charged and the membrane charge is homogeneously distributed in the whole membrane volume
- electroneutrality occurs in the transition region (double layer)
- potential and concentration are radially homogeneous across the pore
- the concentration of ions are only dependent on the coordinate x (cylindrical pores, pore diameter $\ll$ pore length)
- solvent velocity is proportional to the permeate velocity through Eq. (3) and Eq. (8)
- porous support layer of the membrane has a negligible effect on permeate concentration and permeate velocity



The equation system of Nernst-Planck application mode is modified for the electroneutrality condition in membrane since the default application considers electroneutrality in bulk:

$$\sum_{i=1}^{n} z_i c_i + X_M = 0 \tag{9}$$

The general mass balance equation in conservative form in Nernst-Planck application mode is:

$$\frac{dc_i}{dt} + \nabla \cdot \left(-D_{i,P}\nabla c_i - z_i u_i F c_i \nabla \varphi + c_i V\right) = R_i \tag{10}$$

At steady-state without any reaction, Eq. (10) reduces to:

$$\nabla \cdot (-D_{i,P}\nabla c_i - z_i u_i F c_i \nabla \varphi + c_i V) = 0 \tag{11}$$

When the equation is applied to systems having n number of ions, there are $n + 1$ unknowns, which are concentrations of ions 1 to n plus potential $\varphi$. For the solution of the problem, there are n equations of molar flux $J_i$ plus electroneutrality equation. However, the concentration of one component can be determined by using the electroneutrality condition at the end. Therefore, the variables appearing in the boundary conditions of the program are the potential and the concentration of one component in two components system. In the Nernst-Planck application, the mass balance equation for the first species is replaced by the equation of conservation of charge. When

Eq. (11) is weighted with the factor $F\ z_i$ and summed over all ions:

$$\nabla \cdot \left( F \sum_i^n z_i \left( -D_{i,P} \nabla c_i - z_i u_i F c_i \nabla \varphi + c_i V \right) \right) = 0$$

$$\nabla \cdot \left( F \left( \sum_i^n z_i \left( -D_{i,P} \nabla c_i - z_i u_i F c_i \nabla \varphi \right) + \sum_i^n \left( z_i c_i V \right) \right) \right) = 0 \qquad (12)$$

$$\nabla \cdot \left( F \left( \sum_i^n z_i \left( -D_{i,P} \nabla c_i - z_i u_i F c_i \nabla \varphi \right) + V(-X_M) \right) \right) = 0$$

The resulting equation for the conservation of charge is:

$$\nabla \cdot i = 0 \qquad (13)$$

$i$ is defined as the total current density vector.

To sum up, it is ended with two equations, one for the conservation of charge (Eq. (13)) and one for the mass balance equation (Eq. (11)).

In Comsol Multiphysics, equations are applied in the general partial differential equation (PDE) form:

$$\frac{\partial u}{\partial t} + \nabla \cdot \Gamma = S \qquad (14)$$

Implementation of Eq. (11) and Eq. (13) to the equation system of Nernst-Planck application (non-conservative formulation) is shown in the following table for $n$ components system.

The velocity of water $V$ in membrane pores is defined by the help of Darcy's law:

$$v_D = \frac{k \Delta P_e}{\eta \Delta x} \qquad (15)$$

where $v_D$ is the Darcy velocity, which corresponds to the permeate water velocity, $J_W$. In fact, the Hagen-Poiseuille equation is deduced from Darcy's law when the flow within the membrane pores is laminar and the pores are round in shape. Therefore, combining Eq. (3) and Eq. (8) and comparing with Eq. (15) gives permeability as:

$$k = \frac{r_p^2 \varepsilon}{8} \qquad (16)$$

Eq. (16) is used in the program when the program predicts membrane performance. On the other hand, in charge characterization, since experimental data is available, permeability is calculated directly from Darcy's equation:

$$k = \frac{v_D \cdot \eta}{\Delta P_e / \Delta x} \qquad (17)$$

The momentum equation obtained by combining Darcy's law and continuity equation is defined accordingly:

$$\frac{\partial}{\partial t}(\rho\varepsilon) + \nabla\cdot\rho\left(-\frac{k}{\eta}\nabla P\right) = 0 \tag{18}$$

As the system operates at steady state, Eq. (18) reduces to:

$$\nabla\cdot\left(-\rho\frac{k}{\eta}\nabla P\right) = 0 \tag{19}$$

The formulation of Darcy's law in the program occurs similarly as in Nernst-Planck application.

So far the equations and their implementations are introduced. In the binary ion systems considered in this work, the program is solved with the boundary conditions for the concentration of specie 2 and the potential in the Nernst-Planck application mode, whereas the pressure and the velocity boundary conditions in the Darcy's law application mode are applied.

Referring to Fig. 1, for the specie 2, at the interfaces 1 and 4, the concentrations in membrane pores are expressed as a function of bulk concentrations by using Donnan-steric partitioning:

$$\frac{c_i}{C_i} = \phi_i \exp\left(\frac{-z_i F}{R_g T}\Delta\varphi_D\right) \tag{20}$$

Since the value of the Donnan potential at each interface is the same for all ions in the solution, the concentration of species at the boundaries can be derived as a function of membrane charge, bulk concentration, and steric factors. When Donnan potential at a regarding side is equalized for two ions in a single salt system:

$$-\frac{R_g\cdot T}{z_1\cdot F}\cdot\ln\frac{c_1}{\phi_1\cdot C_{1,F}} = -\frac{R_g\cdot T}{z_2\cdot F}\cdot\ln\frac{c_2}{\phi_2\cdot C_{2,F}} \tag{21}$$

$$\left(\frac{c_1}{\phi_1\cdot C_{1,F}}\right)^{1/z_1} = \left(\frac{c_2}{\phi_2\cdot C_{2,F}}\right)^{1/z_2} \tag{22}$$

For NaCl, the subscripts 1 and 2 refer to $Na^+$ and $Cl^-$ ions respectively. Therefore, the above equation leads to:

$$\left(\frac{c_1}{\phi_1\cdot C_{1,F}}\right) = \left(\frac{\phi_2\cdot C_{2,F}}{c_2}\right) \tag{23}$$

For this salt, electroneutrality conditions in membrane and bulk give:

$$c_1 - c_2 + X_M = 0 \tag{24}$$

$$C_1 - C_2 = 0 \tag{25}$$

Substituting Eq. (24) and Eq. (25) in Eq. (23) and rearranging for the component 2 gives:

$$\frac{c_2 - X_M}{\phi_1 \cdot C_{2,F}} = \frac{\phi_2 \cdot C_{2,F}}{c_2} \tag{26}$$

Consequently, at boundary 1, the concentration at the pore inlet for $Cl^-$ in the case of NaCl is derived as:

$$c_2(0) = \frac{X_M + \sqrt{X_M^2 + 4C_F^2\phi_1\phi_2}}{2} \tag{27}$$

Similarly, at permeate side ($x = \Delta x$), $c_2(\Delta x)$ is derived as:

$$c_2(\Delta x) = \frac{X_M + \sqrt{X_M^2 + 4C_P^2\phi_1\phi_2}}{2} \tag{28}$$

Boundary condition equations for other salt types are obtained by following the same method and presented in Table 7. Subscripts 1 and 2 refer to the positive and negative ions, respectively. Equations for $CaCl_2$ and $Na_2SO_4$ require solving of third degree polynomial equations, which can be executed in COMSOL Multiphysics by using the root finding method in one dimension (38).

In the membrane performance prediction program, flux boundary condition is applied at $x = \Delta x$:

$$J_i = V \cdot C_{i,P} \tag{29}$$

Therefore, permeate concentrations should be defined from the relations at boundary $x = \Delta x$ given in Table 7 and should be applied in Eq. (29).

At interfaces 2 and 3, insulation/symmetry boundary condition is applied:

$$J_i \cdot n = 0 \tag{30}$$

$n$ is the outward normal vector to the boundary.

Since at steady state, the net current flow is zero during ion transport, the following boundary condition is applied for the potential boundary condition at all interfaces:

$$-n \cdot i = 0 \tag{31}$$

In the Darcy's law application mode, at boundary 1, the pressure boundary condition is applied:

$$P = P_0 \tag{32}$$

where $P_0$ is the difference between the applied feed pressure minus osmotic feed pressure. Osmotic pressure is calculated from the Van't Hoff equation.

***Table 7.*** Boundary condition equations in Nernst-Planck application mode for charge characterization program of binary systems

| Salt type | At x = 0 → $c_2 = c_20$ | At x = Δx → $c_2 = c_2(\Delta x)$ |
|---|---|---|
| NaCl | $c_2 = \dfrac{X_M + \sqrt{X_M^2 + 4\phi_1\phi_2(C_F)^2}}{2}$ | $c_2 = \dfrac{X_M + \sqrt{X_M^2 + 4\phi_1\phi_2(C_P)^2}}{2}$ |
| $CaCl_2$ | $c_2^3 - X_M c_2^2 - \phi_1 \phi_2^2 C_{2,F}^3 = 0$ | $c_2^3 - X_M c_2^2 - \phi_1 \phi_2^2 C_{2,P}^3 = 0$ |
| $Na_2SO_4$ | $4c_2^3 - 4X_M c_2^2 + X_M^2 c_2 - 4\phi_1^2 \phi_2 C_{2,F}^3 = 0$ | $4c_2^3 - 4X_M c_2^2 + X_M^2 c_2 - 4\phi_1^2 \phi_2 C_{2,P}^3 = 0$ |
| $MgSO_4$ | $c_2 = \dfrac{0.5\,X_M + \sqrt{0.25\,X_M^2 + 4\phi_1\phi_2 C_{2,F}^2}}{2}$ | $c_2 = \dfrac{0.5\,X_M + \sqrt{0.25\,X_M^2 + 4\phi_1\phi_2 C_{2,P}^2}}{2}$ |

At boundary 4, the velocity $V$ inside pore is defined:

$$-n \cdot V = V_0 \tag{33}$$

The velocity boundary condition is expressed using the Solution-Diffusion model water flux equation so that the velocity could be defined as a function of pressures, concentrations, and membrane constant in performance prediction program. Velocity of water in pores is related to permeate water flux using Eq. (8).

$$V_x = \frac{L_P}{\varepsilon}\left[\left(P_F - P_p\right) - \left(\pi_F - \pi_P\right)\right] \tag{34}$$

For the charge characterization program where the value of water flux is assumed to be permeate flux measured, water velocity inside pore is calculated directly from Eq. (8).

The other boundary conditions are insulation/symmetry:

$$-n \cdot V = 0 \tag{35}$$

In the charge characterization program, first, a membrane charge is assumed and the system of equations is solved. The calculated flux for a component $i$ from the program is checked with the expected flux calculated from Eq. (29). The membrane charge is iterated till the calculated flux from the program and from Eq. (29) agrees. In the prediction program, the membrane charge density is a known value determined from adsorption isotherms and concentration of one component in permeate is assumed. Iteration is done till the permeate concentration obtained from Eq. (29) in program agrees with the assumed permeate concentration.



## RESULTS AND DISCUSSIONS

### Membrane Characterization

For the determination of hydrophilic character of the membranes, contact angles were measured and tabulated in Table 8. The values for the sessile drop (1) and captive bubble arose from the average of the values obtained from the measurements performed with three droplets. For each droplet, 10 values were recorded. The sessile drop (2) values are the averages of 6 angle readings. From sessile drop (2) measurements, no concrete values could be read for NF 270 and NF 2 membranes due to the highly hydrophilic character of the membranes and estimated to be less than 10°. The surface roughness, porosity or pore size can hinder the influence of the material itself on the measurements. Therefore, it happened to measure different values for a membrane from the same manufacturer also in (39). Consequently, the measurements in this work were considered to make a comparison

***Table 8.*** Contact angles of the membranes from different measurements

| | Sessile drop (1) | | | Captive bubble | | | |
|---|---|---|---|---|---|---|---|
| Membrane | Adv. | Rec. | Hys. | Adv. | Rec. | Hys. | Sessile drop (2) |
| NF 90 | 12.3 | 0.0 | 12.3 | 0.0 | 0.0 | 0.0 | 30 |
| NF 270 | 8.0 | 0.0 | 8.0 | 0.0 | 0.0 | 0.0 | $<10$ |
| NF 2 | 9.4 | 0.0 | 9.4 | 0.0 | 0.0 | 0.0 | $<10$ |
| NF PES 10 | 57.7 | 10.4 | 47.2 | 48.6 | 17.8 | 30.7 | 50 |

between membranes in terms of their hydrophilic characters. The overall results indicate that NF 2 and NF 270 are the most hydrophilic membranes, followed by NF 90 and NF PES 10, respectively. Similar to the observations made in (39), in which the dependency of the contact angle on the type of membrane active layer material was investigated, the contact angles measured in this study are in the increasing order of polypiperazineamide, polyamide and polyethersulphone.

Arithmetic averages of the absolute values of the surface height deviations ($R_a$) from AFM measurements at different scan sizes are presented in Table 9. There are big differences in roughness at different scan sizes for same samples. An increase in roughness with increasing scan area was also observed in (40), which is the first study investigating this phenomenon. This was related to the dependency of the roughness on the spatial wavelength of the scanned area or the frequency. For a small scan area, only high frequencies are measured. For larger areas, additional lower frequencies are also taken into account giving a higher value roughness. Another explanation was the formation of a fractal structure on the membrane surface when polymers are assembled to nodules. Therefore, at different scan size, different structure topography and thus different roughness is determined. The general order can be summarized as NF 90 > NF 2 > NF 270 > NF PES 10. Hilal et al. (41) utilized AFM for the characterization of NF membranes in terms of their surface roughness, pore size, and pore size distributions. The contact

***Table 9.*** Surface roughnesses (nm) of the membranes at different scan sizes

| | Scan area ($\mu m^2$) | | | | | |
|---|---|---|---|---|---|---|
| Membrane | $1 \times 1$ | $5 \times 5$ | $25 \times 25$ | $50 \times 50$ | $100 \times 100$ | $130 \times 130$ |
| NF 90 | 31.28 | 84.50 | 121.45 | 109.58 | 106.41 | 95.02 |
| NF 270 | 3.02 | 10.16 | 9.52 | 7.65 | 9.19 | 32.58 |
| NF 2 | 3.36 | 8.861 | 9.99 | 12.96 | 28.76 | 35.15 |
| NF PES 10 | 1.25 | 4.27 | 8.42 | 16.25 | 20.55 | 23.34 |

mode measurements at a scan size of $2 \times 2\ \mu m^2$ led to the $R_a$ values, which indicated that NF 90 has the highest roughness (22.7632 nm) followed by NF 270 (3.3611 nm) and NF PES 10 (1.76365 nm). Although a direct comparison is not possible due to different scan sizes, the values are close to the ones or slightly higher than the ones obtained from $1 \times 1\ \mu m^2$ scan size in this work, which indicates qualitative agreement. This parameter can contribute to the membrane performance by affecting the fouling behavior of the membranes. Vrijenhoek et al. (42) investigated the relation between surface morphology and structure to membrane performance for polyamide TFC NF/RO membranes. They have observed a clear correlation between surface roughness and colloidal fouling regardless of physical and chemical operating conditions.

Pure water permeability experiments demonstrated the highest permeabilities for NF 2 (16.7 $L/(m^2\ h\ bar)$) and NF 270 (17.6 $L/(m^2\ h\ bar)$), whereas the lowest ones for NF PES 10 (12.1 $L/(m^2\ h\ bar)$) and NF 90 (13.0 $L/(m^2\ h\ bar)$) were obtained. The repeated experiments for NF 2 and NF 90 using different membrane samples were reproducible. The order of the permeabilities agrees with the ones expected from the manufacturer data of cut-offs and contact angles measured since this characteristic expresses wettability of the membranes and thus differences in permeability.

The zeta potentials calculated from the measurements as a function of pH for KCl, NaCl and $CaCl_2$ salts are presented in Figures 2–4 respectively. In Fig. 2, measurements conducted from neutral to acidic pH as well as acidic to alkaline pH (3–11) are presented. For NF PES 10, there is a weak indication of a plateau, $-33$ mV at pH $> 7$. At plateau, the ionic sites are fully dissociated. The IEP is at pH 2.5. There is no difference between the first (neutral $\rightarrow$ acidic) and second (acidic $\rightarrow$ alkaline) branch

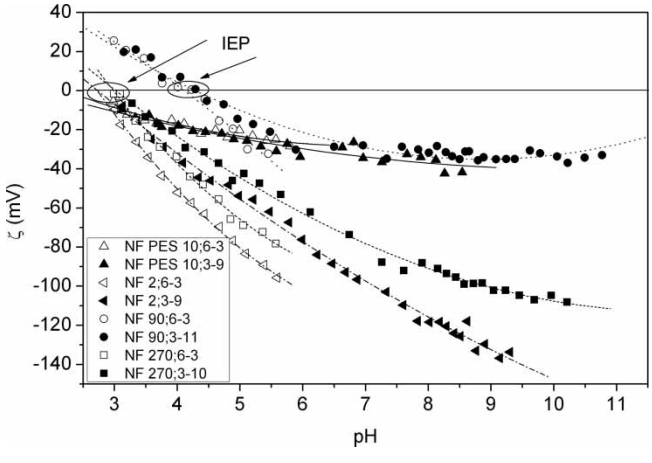


***Figure 2.*** Zeta potentials of the membranes as a function of pH for 0.005 M KCl.

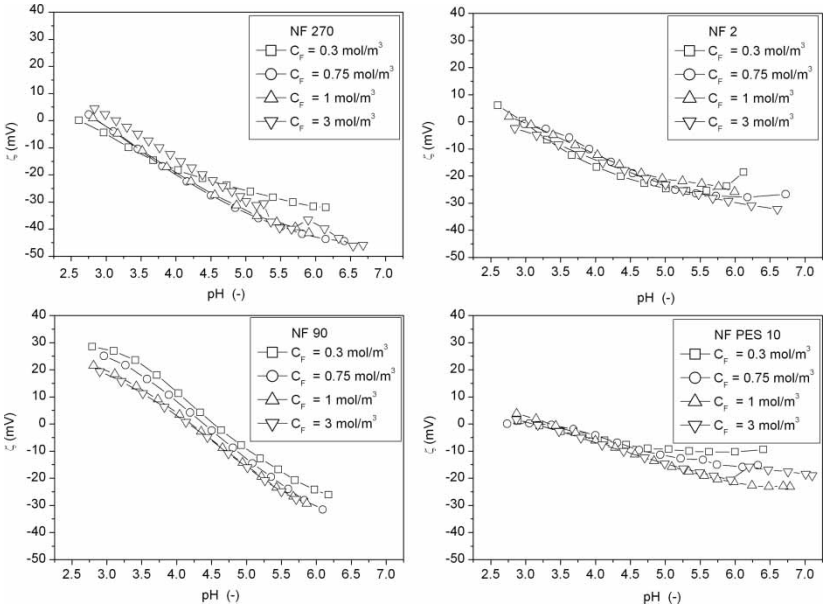


***Figure 3.*** Zeta potentials of the membranes as a function of pH for NaCl solution at different concentrations.

of the measurements. For NF 2 and NF 270, there is no plateau. The IEP is obtained by extrapolation at pH 2.6 for NF 2 and at pH 2.8 for NF 270. There is a large difference between the first and second branch of the measurements for both membranes. For NF 90, below pH $<$ 4.2 (IEP), an instantaneous increase of zeta potential above 0 is observed. There is a plateau of $-33$ mV at pH 7.2 and a remarkable difference between the first and second branch of the measurements. From these observations, it can be concluded that there are roughly two groups showing slightly acidic behavior and an amphoteric behavior. NF PES 10, NF 2 and NF 270 belong to the former and NF 90 to the latter. The first group, isoelectric point (IEP) $<$3 in all cases, indicates the presence of dissociable acidic groups in the surface. In the case of polyamide membranes, no distinct plateau was observed. Hence, the existence of some additional N containing groups can be considered, which turn to be protonated under acidic conditions. The vanishing difference between the first and the second branch of the measurements of NF PES 10 indicates that its surface has no N containing groups. In the second group (amphoteric behavior), the plateau observed at pH 7.2 indicates the presence of dissociable acidic groups on the surface. However, the IEP 4.2 points to the presence of basic groups on the surface at the same time. This is confirmed by the remarkable difference between the first and the second branch of the measurements. In agreement with the

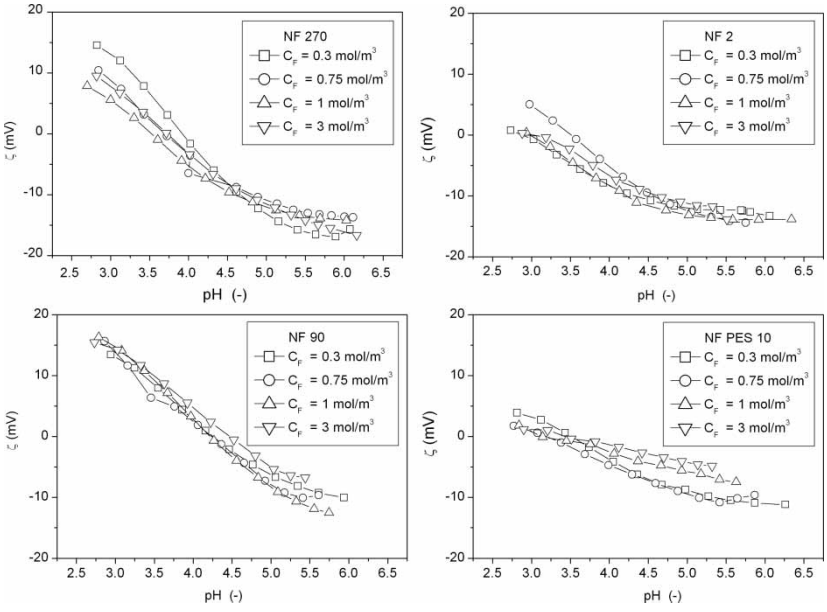


***Figure 4.*** Zeta potentials of the membranes as a function of pH for $CaCl_2$ solution at different concentrations.

suppliers information concerning NF 90, it can be concluded that the surface potential is determined by carboxylic (-COOH) groups and primary amines (-$NH_2$). Amines are protonated below the IEP and carboxylic groups are deprotonated above the IEP. It is observed from plots that at pH around 5–7 which is the pH range of permeation experiments, all membranes investigated have negative zeta potentials and thus negatively charged. It can be observed that zeta potential of NaCl (Fig. 3) is more negative than $CaCl_2$ (Fig. 4), depicting a higher membrane charge. Teixeira et al. (18) and Childress and Elimelech (43) described that divalent cations (such as $Ca^{2+}$ and $Mg^{2+}$) can be adsorbed more readily on the membrane surface which may cause the measured zeta potential less negative than with NaCl solution over the measured pH range.

## Organic Rejections, Pore sizes, and Porosities of the Membranes

Rejections for organic solutions are presented as a function of flux in Fig. 5. Generally, rejection increased with an increase in solute size. One could get the information about the characteristics of the membranes such that NF 90 depicts the highest rejection behavior and NF PES 10 lowest. NF 270 and NF 2 have similar separation and flux performances.

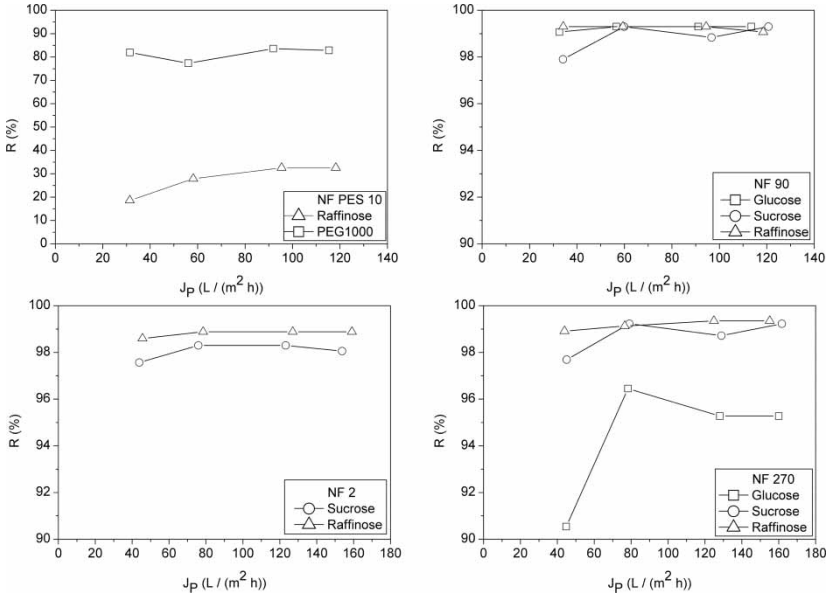


***Figure 5.*** Rejections of organics as a function of permeate flux.

The effective pore radii of the membranes were determined by means of the method introduced in section on effective pore radius and porosity determinations. The results are tabulated in Table 10. Having determined pore sizes, porosities, and permeabilities were calculated and presented in Table 10 as well.

Similar pore sizes for NF 2 and NF 270 membranes and highest pore size for NF PES 10 membrane were expected in view of the manufacturer and characterization data and obtained from simulations. Bowen and Mohammad (14) studied 29 commercial membranes including NF PES 10. All membranes indicated pore radii less than 1 nm, mainly in the range of 0.4 nm–0.7 nm. Wang et al. (11) used a steric-hindrance pore model to calculate the pore size of NF PES 10 membrane. Glycerol, glucose, sucrose, raffinose, and PEG 1000 were used in the experimental analysis. Apart from

***Table 10.*** Pore sizes $r_p$, porosities, $\varepsilon$ and permeabilities, $k$ of the membranes

| Membrane | $r_p$ (nm) | $\varepsilon$ (−) | $k$ ($10^{-21}$ $m^2$) |
|---|---|---|---|
| NF 90 | 0.399 | 0.412 | 8.98 |
| NF 270 | 0.395 | 0.419 | 8.18 |
| NF 2 | 0.392 | 0.467 | 8.19 |
| NF PES 10 | 0.757 | 0.0637 | 4.56 |

PEG 1000 with which the 0.69 nm pore radius was calculated, other organics gave values ranging from 1.12 nm to 1.45 nm. Therefore, the PEG 1000 result was not considered. Nghiem et al. (5, 44) calculated average pore radii of 0.42 nm for NF 270 and 0.34 nm for NF 90 membranes by using organic rejection measurements and a hydrodynamic approach. Hilal et al. (33) used the AFM technique for characterization of NF 90 and NF 270 membranes. They determined lower values: a pore radius of 0.275 nm for NF 90 and 0.35 nm for NF 270. Nevertheless, Bowen et al. (15) stated that AFM might underestimate the pore dimension due to the convolution effects between tip and pore. In addition, scan speed and cantilever type can contribute to imaging artefacts (41). It was also not expected higher pore size estimation for NF 90 than NF 270 membrane in our calculations. However, very high rejections were obtained with NF 90 membrane and thus low permeate concentrations at undetectable limits. Therefore, permeate samples must have been concentrated. In addition, only one feed sample for each experiment was taken, which was a critical point since it might be taken from the feed tank at a position which might not reflect experimental condition. Therefore, rejections data were influenced at every measurement point when an error was encountered regarding feed stream. Thus, simulation results were significantly affected.



## Single Salt Rejections

The rejections as a function of feed concentrations are presented in Fig. 6. Pure water permeabilities measured before each experiment are presented in the diagrams as well. The differences in pure water permeabilities might affect the rejection performance as well. It is widely observed that the higher the pure water permeability the lower is the rejection. However, there is no such general rule. All TFC membranes depicted high rejections for sulphate salts. Since sulphate is a divalent coion, a strong electrostatic exclusion from the membrane occurred.

According to the Donnan theory, at equilibrium concentrations the rejection sequence should be $R(Na_2SO_4) > R(MgSO_4) = R(NaCl) > R(CaCl_2)$ for a negatively charged membrane and vice versa for a positively charged membrane. Accordingly, referring to Fig. 6 some membranes revealed that the rejection mechanism was governed by the Donnan exclusion and some by a combination of Donnan and steric effects. For NF PES 10, the results are in accordance with Donnan exclusion. Rejections decreased with increasing concentration. One explanation for this behavior is the increasing coion distribution between the membrane and the solution, which leads to a lower rejection. In addition, the Debye length decreases with increasing feed concentration, which accelerates the shielding of membrane charge by counterions. The thinner the electric double layer (Debye length), the easier it is to shield the wall potential of the membrane.

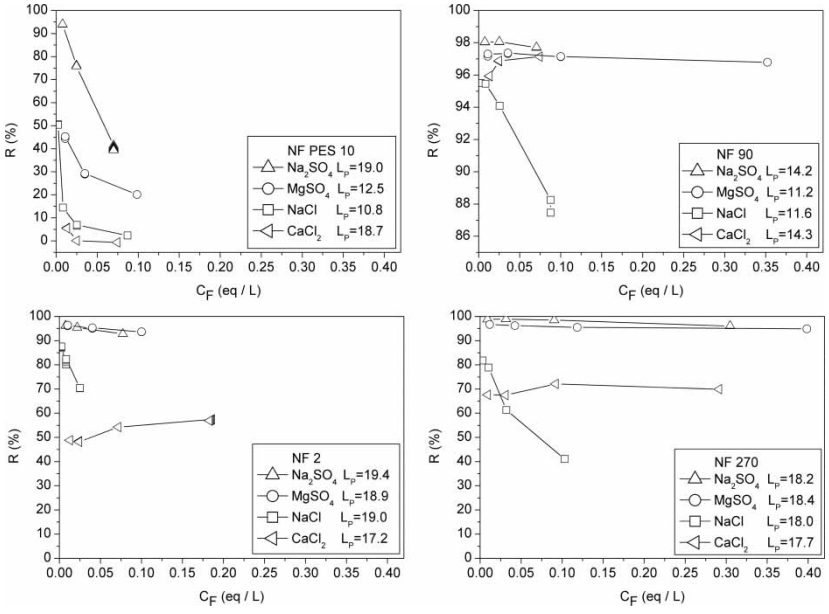


***Figure 6.*** Rejections of salts as a function of feed concentration.

Consequently, coions are excluded worse, which leads to a lower rejection. This effect of concentration on rejection was observed for all membranes apart from $CaCl_2$ salt for some membranes. It can be foreseen that the rejection of $Na_2SO_4$ would be equal or less than the $MgSO_4$ rejection at higher concentrations. This probably indicates that transport by diffusion starts dominating as a consequence of decreasing electrostatic exclusion of the anions due to the shielding of the membrane potential by counterions.

The same experiments with NF 90 membrane resulted in retentions for all salts above 87%. The retention sequence was $R(Na_2SO_4) > R(MgSO_4) > R(CaCl_2) > R(NaCl)$ indicating both the charge and the steric effects on the rejection behavior.

The experiments performed with NF 2 demonstrated that the rejection mechanism was governed by charge. Slightly higher rejections for the $MgSO_4$ can be ascribed to the measurement errors. Rejection measurements with NF 270 delivered similar results to NF 2 apart from the lower NaCl rejection than $CaCl_2$ rejection which can not be explained through alone charge effects. Higher rejection for $CaCl_2$ than NaCl was explained through the less shielding of membrane charge (high Debye length) by $Ca^{2+}$ ions due to the steric effect (45). That is to say, higher stokes radius of $Ca^{2+}$ led to a lower concentration in the membrane. Therefore, although the Debye length at the same concentrations was lower than the NaCl one, not enough $Ca^{2+}$ ions in the pores existed for the shielding of the membrane potential,

which led to higher rejections with $CaCl_2$ than NaCl salt. The increase in $CaCl_2$ rejection along with feed concentration was observed not only for NF 2 membrane but also for NF 270 and NF 90 membranes, which could not be explained through Donnan effect. The same rejection behavior for $CaCl_2$ was observed also in (19, 24). No explanation could be given in (19) apart from probable steric effects due to large hydrated radius of $Ca^{2+}$. Hagmeyer et al. (24) supposed that membranes possess higher charge at increasing concentrations so that higher rejections for $CaCl_2$ at higher concentrations were observed. However, the zeta potential measurements did not confirm this assumption. These results were implemented through higher hydration energies of divalent cations than monovalent cations, which led to stronger surface forces with the membrane and formed stable complexes with membrane functional groups (46). Thus, the membrane charge and its effect on rejection decreased. In addition, the effect of drag forces on divalent cations due to convective flux decreased. Consequently, rejection happened through steric hindrance, which stayed high for divalent cations and correspondingly for $CaCl_2$ salt due to the electroneutrality condition. Simply expressed, highly hydrated ion has high hydration energy and thus high rejection. The rejection sequence of different 2-1 salts in comparison to 1-1 salts confirmed this conclusion in (46, 47).



## pH Effect

Figure 7 depicts rejection profiles of membranes with various single salts as a function of pH. It is observed that the negative membrane charge character leads to decreasing rejections of NaCl, $Na_2SO_4$, and $MgSO_4$ at decreasing pH. Exceptions are with the $CaCl_2$ solution, where an increase in rejection with decreasing pH is observed. Similar rejection behaviors as a function of pH are observed in (48) for NaCl (decreasing rejection at decreasing pH in acidic range, minimum and increasing rejection at decreasing pH in basic range), for $MgCl_2$ (increasing rejection at decreasing pH in acidic range, maximum, slightly decreasing rejection at decreasing pH in basic range), and for $Na_2SO_4$ (high and slightly increasing rejection at increasing pH). Furthermore, it is obvious that the pH effect has stronger influence on the rejections of NaCl and $CaCl_2$ salts than $Na_2SO_4$ and $MgSO_4$ salts. Referring to Fig. 3 and Fig. 4, since membranes are negatively charged in this pH range, electrostatic exclusion is high for sulphate salts and does not affected as much as NaCl and $CaCl_2$ salts. Childress et al. (26) investigated the membrane performance and charge as a function of pH for TFC NF 55 membrane, which has a similar polymeric structure to NF 90 membrane. In similar to the flux behavior of NF 270 for NaCl salt (Fig. 8), where a maximum in flux is observed close to IEP, a peak in flux at IEP was obtained for NF 55 as well. This is attributed to the possibly occurred mechanisms such as increased pore size due to conformational

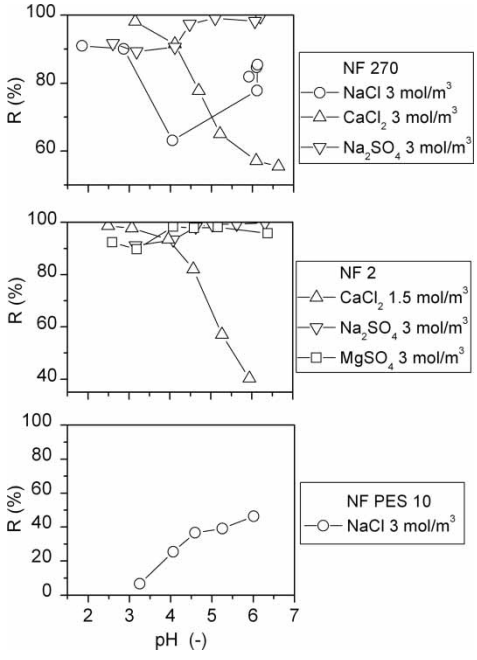


***Figure 7.*** Rejection of salts as a function of pH for different membranes.

changes of the cross-linked membrane polymer structure, increased apparent water permeability due to decreased electroviscous effect, and increased net driving pressure due to decreased osmotic pressure at the membrane surface at IEP. These mechanisms are explained in detail in (26). Similarly, a minimum in total molar rejection (total number of moles of all ions, $H^+$, $Cl^-$, $Na^+$) at IEP was observed, which is a consequence of lacking coion exclusion due to zero membrane charge. A similar phenomenon is encountered with NF 270 and NaCl salt in our work (Fig. 7). However, when the conductivity rejection was concerned, a local minimum of rejection at IEP (pH = 5) was detected, which increased from pH 5 to 4 and decreased dramatically towards pH 3 because of extensive proton passage through the membrane (26). When the conductivity rejection is considered, rejection decreases as pH decreases and reaches negative values in our work. This is attributed to high $H^+$ permeation in the presence of $Na^+$ ions due to its higher ionic mobility and lower size. Since molar conductance of $H^+$ is higher than $Na^+$ and $Cl^-$ ions, it contributes significantly to permeate conductivity (26). Consequently, the negative conductivity rejection was observed.

At pH > 5, NF 270 indicated rejection order of Donnan mechanism and at pH > 4, the NF 2 membrane showed rejections in agreement for a

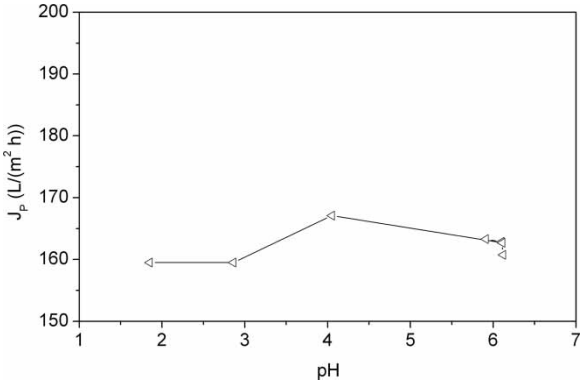


***Figure 8.*** Permeate flux as a function of pH for NF 270 membrane with NaCl solution.



negatively charged membrane. As realized, the order of separation of salts depends strongly on solution pH. Consequently, the separation performance of the membranes for the related salts can be enhanced by adjusting the pH of the solution.

## Effective Membrane Charge Density and Membrane Performance

In many studies it was found that the charge density depends on salt type and salt concentration (14, 16, 21, 47). This dependency is expressed by adsorption isotherms. A linear dependency between membrane charge and feed concentration is achieved by logarithmic scaling of the Freundlich isotherm:

$$\log|X_M| = s \log C_F + q \tag{36}$$

The logarithmic effective membrane charge densities calculated with different salt types are presented in Fig. 9 as a function of logarithmic feed concentrations. It is observed that the membrane charge increases with increasing salt concentration. The isotherm constants are presented in Table 11. The order of adsorption was $NaCl > Na_2SO_4 > MgSO_4$.

Eq. (36) can also be written as:

$$X_M = r(C_F)^s \tag{37}$$

where $\log r = q$. From this equation, the ratio $X_M/C_F$ can be written as:

$$\frac{X_M}{C_F} = r(C_F)^{s-1} \tag{38}$$

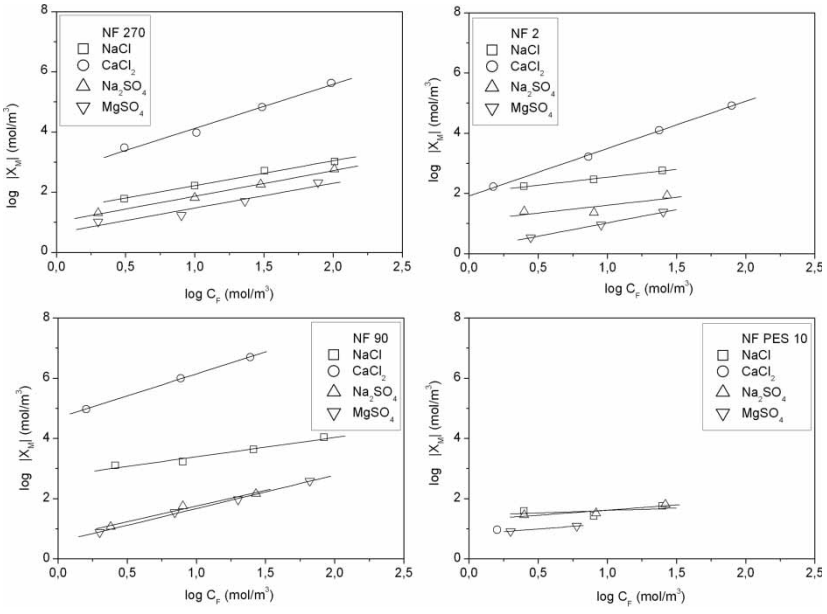


***Figure 9.*** Adsorption isotherms of membranes for different salts.

The profile of $X_M/C_F$ ratio and $C_F$ can be investigated by deriving the above equation with respect to $C_F$, which gives Eq. (39):

$$\frac{d(X_M/C_F)}{d\,C_F} = r(s-1)\,(C_F)^{s-2} \tag{39}$$

If $(s-1)$ is negative, it means that the effect of charge the decreases with increasing concentration and vice versa. If the $(s-1)\approx 0$, the charge effect

***Table 11.*** Constants in Freundlich isotherms

| | Salt | | | | | | | |
|---|---|---|---|---|---|---|---|---|
| | $Na_2SO_4$ | | $MgSO_4$ | | NaCl | | $CaCl_2$ | |
| Membrane | *s* | *q* | *s* | *q* | *s* | *q* | *s* | *q* |
| NF 270 | 0.85 | 1.02 | 0.83 | 0.65 | 0.83 | 1.4 | 1.47 | 2.65 |
| NF 2 | 0.52 | 1.09 | 0.88 | 0.13 | 0.53 | 2 | 1.57 | 1.92 |
| NF 90 | 1.04 | 0.71 | 1.11 | 0.56 | 0.64 | 2.8 | 1.46 | 4.68 |
| NF PES 10 | 0.34 | 1.28 | 0.36 | 0.81 | 0.16 | 1.44 | n.p | n.p |

n.p = not performed.

remains constant at increasing concentration due to increasing shielding effect. From the *s* values in Table 11, it is concluded that unlike other salts, $CaCl_2$ solution shows an increase of charge effect with increasing concentration. However, it has to be mentioned that the quantity of $X_M$ obtained from charge characterization programs do not necessarily reflect the true physical charge density in the membrane. But, it is more a fitting parameter that corresponds to not only charge density, but also to other various phenomena, such as dielectric exclusion, ion-ion interactions, and the non ideal behavior of the solution. For the amphoteric NF 90 membrane, charge effects are negligible for $Na_2SO_4$ and $MgSO_4$ salts.

By means of the adsorption isotherms, the rejections predicted from the simulations as a function of feed concentrations are presented in Fig. 10. From the prediction program developed, the effects of process parameters or membrane properties to the separation performance can be investigated. Figure 11 shows the plot of rejection versus volumetric water flux at constant feed concentration and constant membrane charge density for different salt solutions and NF 270 membrane. It is observed that with increasing water flux, rejection reaches a maximum limiting value. This result is in accordance with experimental results found in previous works (20, 24, 25).

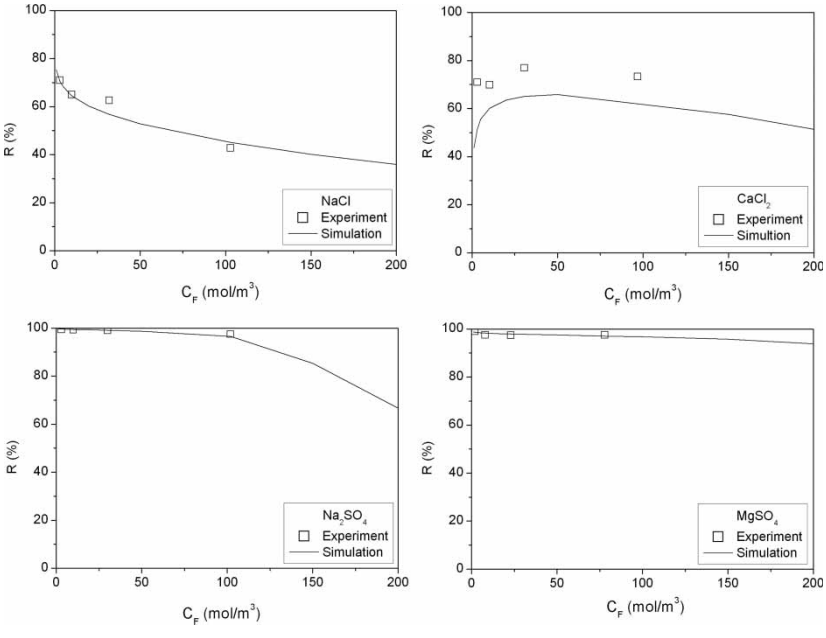


***Figure 10.*** Comparison of rejection of single salt solutions obtained from experiments and simulations for NF 270 membrane.

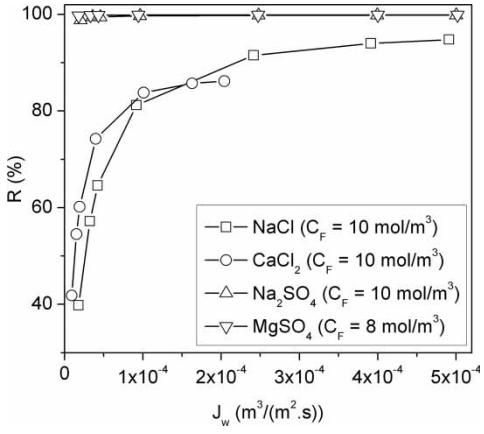


***Figure 11.*** Rejections of salts as a function of water flux for NF 270 membrane.



## Evaluation of the Transport Mechanisms

The calculated ion concentrations of $Na^+$ and $Cl^-$ at both membrane interfaces are listed in Table 12. It is observed that the concentration of counterion ($Na^+$) in the membrane increases significantly compared to its concentration in bulk. A low concentration of coion ($Cl^-$) exists in the membrane and the electroneutrality condition in the membrane volume is maintained.

From transport mechanism investigations it is observed that diffusion, convection, and electromigration of coions act towards the permeate side. For counterions, electromigration occurs from permeate to the feed side due to the higher potential on the permeate side. Figure 12 shows that all transport mechanisms (diffusion, convection, and electromigration) increase with increasing concentration. As the concentration increases, the

***Table 12.*** Ion concentrations on the interfaces between bulk solution and membrane surface for NaCl solution and NF 270 membrane

| At feed – membrane interface x = 0 | | | At permeate – membrane interface x = Δx | | | |
|---|---|---|---|---|---|---|
| $C_F$ (mol/m$^3$) | $c_+(0)$ (mol/m$^3$) | $c_-(0)$ (mol/m$^3$) | $C_P$ (mol/m$^3$) | $c_+(\Delta x)$ (mol/m$^3$) | $c_-(\Delta x)$ (mol/m$^3$) | $X_M$ (mol/m$^3$) |
| 3.1 | 60.522 | 0.022 | 0.9 | 60.502 | 0.002 | −60.5 |
| 10.0 | 163.084 | 0.084 | 3.5 | 163.010 | 0.010 | −163 |
| 32.0 | 510.274 | 0.274 | 12.0 | 510.038 | 0.038 | −510 |
| 103.0 | 1029.405 | 1.405 | 59.0 | 1028.461 | 0.461 | −1028 |

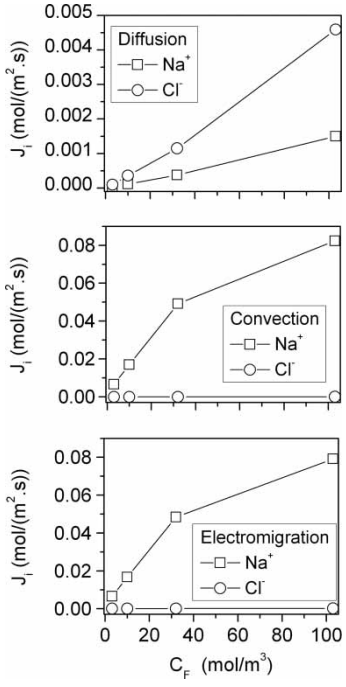


***Figure 12.*** Effects of concentration on transport mechanisms for NaCl salt and NF 270 membrane.



concentration gradient increases as depicted in Table 12 and consequently the diffusive flux also increases. Convective flux is influenced by ion concentration and velocity, while the electromigrative flux is influenced by ion concentration and potential gradient. Therefore, the convective transport is higher for $Na^+$ (higher concentration) than $Cl^-$ ions. Although the concentration gradients inside the membrane are the same at each feed concentration, a higher diffusion coefficient of $Cl^-$ leads to a higher diffusive transport.

Contribution of each term to mass transport is represented in terms of its percentage of the total ion flux as seen in Fig. 13 for NaCl salt in NF 270. In this work, an analysis of diffusive, convective, and electromigrative terms are performed for all single salts and with membranes NF 270, NF 2, and NF 90. It is found that the contribution of each term does not vary too much and is similar with Fig. 13. For coion, the most significant transport mechanism inside the membrane is diffusion, while the contribution of convection and electromigration are below 10%. For the counterion, the contribution of convection and electromigration are equally significant whereas the diffusion is less pronounced. All three transport mechanisms are important and determine mass transport of ions inside the membrane. Therefore, modelling of mass transport in nanofiltration membranes should take all these mechanisms into account.

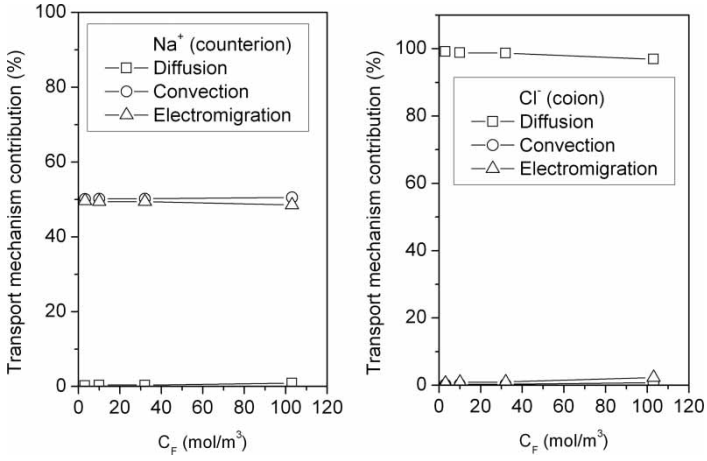


***Figure 13.*** Contribution of transport mechanisms for NaCl in NF 270 membrane.



## CONCLUSIONS

The present paper introduced a comprehensive characterization study of nanofiltration membranes in terms of morphology/charge properties and filtration performances. Zeta potential measurements exhibited that membranes are negatively charged and NF 90 has an amphoteric character. From the rejection measurements, selective characters of the membranes were investigated both qualitatively and quantitatively. In view of the qualitative aspect, it is concluded that the rejection mechanism is governed by a negative charge for NF 2 and NF PES 10 membranes, combined with steric effects for NF 270 and NF 90 membranes. NF 2 and NF 270 proved similarity in terms of morphology and performance. Performances of the membranes were significantly influenced by solution pH.

A program based on the ENP equation was implemented in software COMSOL Multiphysics, which eliminated effort demanding program code writing. The program enabled the ease of implementation of boundary conditions. From the charge characterization program using single salts experimental data it was found out that except for $CaCl_2$, the ratio of the membrane charge to feed concentration decreased with increasing feed concentration, which indicated the weakening of electrostatic interactions at higher concentrations. Transport mechanisms for ions inside the membrane could be identified in a straightforward manner. The model presented can be used as a basic means for multicomponent simulations in NF membranes, whereas the new implementations of the boundary conditions for the feed and permeate sides are unavoidable.

## LIST OF SYMBOLS

| | |
|---|---|
| $c_i$ | concentration of ion i in the membrane (mol/m$^3$) |
| $c_+(0)$ | concentration of positive ion at the pore inlet (mol/m$^3$) |
| $c_+(\Delta x)$ | concentration of positive ion at the pore outlet (mol/m$^3$) |
| $c_-(0)$ | concentration of negative ion at the pore inlet (mol/m$^3$) |
| $c_-(\Delta x)$ | concentration of negative ion at the pore outlet (mol/m$^3$) |
| d | thickness of the oriented solvent layer (m) |
| $C_F$ | feed concentration (mol/m$^3$) |
| $C_P$ | permeate concentration (mol/m$^3$) |
| $D_i$ | bulk diffusion coefficient of component i (m$^2$/s) |
| $D_{i,P}$ | hindered diffusivity of ion i in membrane (m$^2$/s) ($D_i^* = D_i \cdot K_{d,i} \cdot \eta_o/\eta$) (21)) |
| $D_p$ | hindered diffusivity of uncharged solute in membrane (m$^2$/s) |
| e | electronic charge (1.60218 $10^{-19}$ C) |
| $F$ | Faraday constant (96487 C/mol) |
| i | total current density (C/(m$^2$ s)) |
| $J_i$ | ion flux (mol/(m$^2$ s)) |
| $J_P$ | permeate flux (L/(m$^2$ h)) |
| $J_w$ | water flux based on membrane area (m/s) |
| $k$ | permeability (m$^2$) |
| $k_B$ | Boltzman constant (1.38066 $10^{-23}$ J/K) |
| $K_d$ | hindrance factor for diffusion ($Kc = 1.0 - 2.30\lambda + 1.154^2 + 0.224^3$) (16)) |
| $L_P$ | membrane constant (m/(s Pa)) |
| $r_i$ | size of ion i (m) |
| $r_p$ | effective pore radius (m) |
| $r_s$ | stokes radius of ions or solutes (m) |
| s | constant of Freundlich isotherm |
| P | pressure (Pa) |
| $P_F$ | feed side pressure (Pa) |
| $P_P$ | permeate side pressure (Pa) |
| $Pe$ | Peclet number |
| R | measured rejection (%) |
| $R_g$ | gas constant (J/(mol K)) |
| $R_{calc}$ | calculated rejection |
| $R_i$ | reaction term (mol/(m$^3$ s)) |
| q | constant of Freundlich isotherm |
| $S$ | source term (mol/(m$^3$ s)) |
| $T$ | temperature (K) |
| $u_i$ | mobility of ion i (mol/(kg s)) |
| $v_D$ | Darcy velocity (m/s) |
| $V$ | velocity in pore (m/s) |
| $V_x$ | velocity in pore in x direction (m/s) |
| $X_M$ | effective membrane charge (mol/m$^3$) |

| | |
|---|---|
| $z_i$ | valence of ion |
| $z_+$ | positive ion valance |
| $z_-$ | negative ion valance |
| $\Gamma$ | flux vector |
| $\Delta$ | difference |
| $\Delta P_e$ | effective pressure driving force (Pa) |
| $\pi_F$ | feed side osmotic pressure (Pa) |
| $\pi_P$ | permeate side osmotic pressure (Pa) |
| $\Delta x$ | membrane active layer thickness (m) |
| $\varphi$ | potential in axial direction inside the membrane (V) |
| $\varphi_{B,F}$ | potential in feed bulk (V) |
| $\varphi_{B,P}$ | potential in permeate bulk (V) |
| $\varphi_{M,F}$ | potential in membrane on feed side (V) |
| $\varphi_{M,P}$ | potential in membrane on permeate side (V) |
| $\Delta\varphi_D$ | Donnan potential (V) |
| $\Delta\varphi_{D,0}$ | Donnan potential at feed side (V) |
| $\Delta\varphi_{D,\Delta x}$ | Donnan potential at permeate side (V) |
| $\gamma$ | activity coefficient |
| $\varepsilon$ | porosity |
| $\varepsilon_o$ | permittivity of free space ($8.85419\ 10^{-12}\ C^2/(J\ m)$) |
| $\varepsilon_b$ | bulk dielectric constant |
| $\zeta$ | zeta potential (V) |
| $\eta$ | solvent viscosity in pores (Pa s) ($\eta = \eta_o(1 + 18(d/r_p) - 9(d/r_p)^2)$ from (**21**)) |
| $\eta_o$ | bulk viscosity ($Pa \cdot s$) |
| $\phi$ | steric partition coefficient |
| $\lambda$ | ratio of ionic or solute radius to pore radius |
| $\rho$ | density ($kg/m^3$) |
| $\nabla$ | Nabla operator |



## ACKNOWLEDGEMENTS

The Graduiertenkolleg, under the sponsorship of the Deutsche Forschungsgemeinschaft (DFG), is gratefully acknowledged for offering a PhD fellowship to G. Artuğ. GKSS research center is thanked for their contributions. The authors would like to thank the students Alp Ergünsel, Yvonne Evers, and Aferdita Golbach for their involvement. Furthermore, Filmtec, Sepro, and Microdyn-Nadir are also thanked for providing membrane samples.

## REFERENCES

1. Mänttäri, M., Nuortila-Jokinen, J., and Nyström, M. (1997) Evaluation of nanofiltration membranes for filtration of paper mill total effluent. *Filtration and Separation,* 275–280.

2. Mänttäri, M., Pekuri, T., and Nyström, M. (2004) NF 270, a new membrane having promising characteristics and being suitable for treatment of dilute effluents from the paper industry. *J. Membrane Science*, 242: 107–116.
3. Atra, R., Vatai, G., Bekassy-Molnar, E., and Balint, A. (2005) Investigation of ultra- and nano-filtration for utilization of whey protein and lactose. *J. Food Engineering*, 3: 325–332.
4. Vourch, M., Ballannec, B., Chaufer, B., and Dorange, G. (2005) Nanofiltration and reverse osmosis of model process waters from the dairy industry to produce water for reuse. *Desalination*, 172: 245–256.
5. Nghiem, L.D., Schäfer, A.I., and Elimelech, M. (2005) Pharmaceutical retention mechanisms by nanofiltration membranes. *Environmental Science & Technology*, 39: 7698–7705.
6. Yoon, Y., Westerhoff, P., Snyder, S.A., and Wert, E.C. (2006) Nanofiltration and ultrafiltration of endocrine disrupting compounds, pharmaceuticals and personal care products. *J. Membrane Science*, 270: 88–100.
7. Bes-Piá, A., Iborra-Clar, M.I., Iborra-Clar, A., Mendoza-Roca, J.A., Cuartas-Uribe, B., and Alcaina-Miranda, M.I. (2005) Nanofiltration of textile industry wastewater using a physicochemical process as a pre-treatment. *Desalination*, 178: 343–349.
8. Hassan, A.M., Farooque, A.M., and Jamaluddin, A.T.M. (2000) A demonstration plant based on the new NF-SWRO process. *Desalination*, 131: 157–171.
9. Al-Sofi, M.A., Hassan, A.M., Hamed, O.A., Dalvi, A.G.I., Kither, M.N.M., Mustafa, G.M., and Bamardouf, K. (2000) Optimization of hybridized seawater desalination process. *Desalination*, 131: 147–156.
10. Matsuura, T. (2001) Progress in membrane science and technology for seawater desalination-a review. *Desalination*, 134: 47–54.
11. Wang, K.Y. and Chung, T.S. (2005) The characterization of flat composite nanofiltration membranes and their applications in the separation of Cephalexin. *J. Membrane Science*, 247: 37–50.
12. Bouchoux, A., Roux-de Balmann, H., and Lutin, F. (2005) Nanofiltration of glucose and sodium lactate solutions variation of retention between single and mixed-solute solutions. *J. Membrane Science*, 258: 123–132.
13. Bowen, W.R. and Mohammad, A.W. (1998) A theoretical basis for specifying nanofiltration membranes-dye/salt/water streams. *Desalination*, 117: 257–264.
14. Bowen, W.R. and Mohammad, A.W. (1998) Characterization and prediction of nanofiltration membrane performance-a general assessment. *IChemE.,* November 76 Part A: 885–893.
15. Bowen, W.R., Mohammad, A.W., and Hilal, N. (1997) Characterization of nanofiltration membranes for predictive purposes-use of salts, uncharged solutes and atomic force microscopy. *J. Membrane Science*, 126: 91–105.
16. Bowen, W.R. and Mohammad, A.W. (1998) Diafiltration by nanofiltration: Prediction and optimization. *AIChE J.*, 44 (8): 1799–1810.
17. Schaep, J. and Vandecasteele, C. (2001) Evaluating the charge of nanofiltration membranes. *J. Membrane Science*, 188: 129–136.
18. Teixeira, M.R., Rosa, M.J., and Nyström, M. (2005) The role of membrane charge on nanofiltration performance. *J. Membrane Science*, 265: 160–166.
19. Berg, P., Hagmeyer, G., and Gimbel, R. (1997) Calculation of salt rejections through nanofiltration membranes taking into account the diffusion, the convection and electrostatic interactions. *Vom Wasser*, 89: 227–245.

20. Bowen, W.R. and Mukhtar, H. (1996) Characterisation and prediction of separation performance of nanofiltration membranes. *J. Membrane Science*, 112: 263–274.
21. Bowen, W.R. and Welfoot, J.S. (2002) Modelling the performance of membrane nanofiltration- critical assessment and model development. *Chemical Engineering Science*, 57: 1121–1137.
22. Schaep, J., Vandecasteele, C., Mohammad, A.W., and Bowen, W.R. (2001) Modelling the retention of ionic components for different nanofiltration membranes. *Separation and Purification Technology*, 22–23: 169–179.
23. Peeters, J.M.M., Mulder, M.H.V., and Strathmann, H. (1999) Streaming potential measurements as a characterization method for nanofiltration membranes. *Colloids and Surfaces*, 150: 247–259.
24. Hagmeyer, G. and Gimbel, R. (1998) Modelling the salt rejection of nanofiltration membranes for ternary ion mixtures and for single salts at different pH values. *Desalination*, 117: 247–256.
25. Hagmeyer, G. and Gimbel, R. (1999) Modelling the salt rejection of nanofiltration membranes using zeta potential measurements. *Separation and Purification Technology*, 15: 19–30.
26. Childress, A.E. and Elimelech, M. (2000) Relating nanofiltration membrane performance to membrane charge (electrokinetic) characteristics. *Environmental Science & Technology*, 34: 3710–3716.
27. Werner, C., Jacobasch, H.J., and Reichelt, G. (1995) Surface characterization of hemodialysis membranes based on streaming potential measurements. *J. Biomaterial Science*, 7: 61–76.
28. Elimelech, M., Chen, W.H., and Waypa, J.J. (1994) Measuring the zeta (electrokinetic) potential of reverse osmosis membranes by a streaming potential analyzer. *Desalination*, 95: 269–286.
29. Bandini, S., Drei, J., and Vezzani, D. (2005) The role of pH and concentration on the ion rejection in polyamide nanofiltration membranes. *J. Membrane Science*, 264: 65–74.
30. Bowen, W.R., Welfoot, J.S., and Williams, P.M. (2002) Linearized transport model for nanofiltration: Development and assessment. *AlChE J.*, 48 (4): 760–773.
31. Mohammad, A.W. and Takriff, M.S. (2003) Predicting flux and rejection of multicomponent salts mixture in nanofiltration membranes. *Desalination*, 157: 105–111.
32. Ahmad, A.L., Chong, M.F., and Bhatia, S. (2005) Mathematical modelling and simulation of the multiple solutes system for nanofiltration process. *J. Membrane Science*, 253: 105–111.
33. Hilal, N., Al-Zoubi, H., Mohammad, A.V., and Darwish, N.A. (2005) Nanofiltration of highly concentrated salt solutions up to seawater salinity. *Desalination*, 184: 315–326.
34. http://www.dow.com/PublishedLiterature/dh_0384/09002f13803841ae.pdf?filepath=liquidseps/pdfs/noreg/609-02004.pdf&fromPage=GetDoc.
35. Nightingale, E.R. (1959) Phenomenological theory of ion solvation. Effective radii of hydrated ions. *J. Phys. Chem.*, 63 (9): 1381–1387.
36. Peeters, J.M. M. (1997) *Characterization of Nanofiltration Membranes, in Chemical Technology*; University of Twente: Enschede.
37. Freger, V. (2004) Swelling and morphology of the skin layer of polyamide composite membranes: an atomic force microscopy study. *Environmental Science & Technology*, 38: 3168–3175.

38. Zimmerman, W.B.J. (2004) *Process Modelling and Simulation with Finite Element Methods*; World Scientific: UK, 24–25.
39. Wendler, B. (2003) *Nanofiltration von Tensidlösungen-Modellierung und Experimentelle Analyse*; Shaker: Berlin.
40. Boussu, K., Van Der Bruggen, B., Volodin, A., Sanuwaert, J., and Van Haesendock, C. (2005) Roughness and hydrophobicity studies of nanofiltration membranes using different modes of AFM. *Journal of Colloid and Interface Science*, 286: 632–638.
41. Hilal, N., Al-Zoubi, H., Darwish, N.A., and Mohammad, A.W. (2005) Characterisation of nanofiltration membranes using atomic force microscopy. *Desalination*, 177: 187–199.
42. Vrijenhoek, E.M., Hong, S., and Elimelech, M. (2001) Influence of membrane surface properties on initial rate of colloidal fouling of reverse osmosis and nanofiltration membranes. *J. Membrane Science*, 188: 115–128.
43. Childress, A.E. and Elimelech, M. (1996) Effect of solution chemistry on the surface charge of polymeric reverse osmosis and nanofiltration membranes. *J. Membrane Science*, 119: 253–268.
44. Nghiem, L.D., Schäfer, A.I., and Elimelech, M. (2004) Removal of natural hormones by nanofiltration membranes: measurement, modelling, and mechanisms. *Environmental Science & Technology*, 38: 1888–1896.
45. Schneider, G. (1994) *Trenverhalten von Nanofiltrationsmembranen*; Shaker: Aachen.
46. Paugam, L., Taha, S., Dorange, G., Jaouen, P., and Quéméneur, F. (2004) Mechanism of nitrate ions transfer in nanofiltration depending on pressure, pH, concentration and medium composition. *J. Membrane Science*, 231: 37–46.
47. Afonso, M.D. and Pinho, M.N. d. (2000) Transport of $MgSO_4$, $MgCl_2$, and $Na_2SO_4$ across an amphoteric nanofiltration membrane. *J. Membrane Science*, 179: 137–154.
48. Xu, Y. and Lebrun, R.E. (1999) Investigation of the solute separation by charged nanofiltration membrane: effect of pH, ionic strength and solute type. *J. Membrane Science*, 158: 93–104.